RSC Advances

ROYAL SOCIETY OF CHEMISTRY

www.rsc.org/advances

Low-cost and Large-scale Fabrication of Superhydrophobic 5052 Aluminum Alloy Surface with Enhanced Corrosion Resistance

Xue-Wu Li,[†] Qiao-Xin Zhang,*[,†] Zheng Guo,[‡] Jin-Gui Yu,[†] Ming-Kai Tang,[†] and Xing-Jiu Huang*[,†,‡]

[†]School of Mechanical and Electronic Engineering, Wuhan University of Technology, 122 Luoshi Road, Wuhan, 430070, P. R. China

[‡]Research Center for Biomimetic Functional Materials and Sensing Devices, Institute of Intelligent Machines, Chinese Academy of Sciences, Hefei, 230031, P. R. China

*Address correspondence to Q.-X. Zhang, X.-J. Huang.

E-mail: zhangqx@whut.edu.cn(Q.X.Z); xingjiuhuang@iim.ac.cn (X.J.H).

Tel.: +86-551-5591142; fax: +86-551-5592420.

ABSTRACT

Superhydrophobic 5052 aluminum alloy substrates with an excellent corrosion resistance have been fabricated by a simple and low-cost method of acid treatments and modification of fluoroalkyl-silane combined with surface passivation. Via an etching process with hydrochloric acid, hierarchical convex-concave micro/nano-structures have been formed on 5052 aluminum alloy surfaces. Then they were covered with a flocculent layer after passivated with potassium permanganate. The wettability and corrosion resistance of as-prepared substrates have been systematically investigated. The results indicate that aluminum alloy substrates with the etching time of 5 min and passivation time of 180 min exhibit a well superhydrophobicity with a water contact angle of 153±0.7°. In addition, their corrosion resistances are also explored by potentiodynamic polarization curves and electrochemical impedance spectroscopy. Clearly, corrosion resistance of as-prepared aluminum alloy substrates has been greatly enhanced, which will be positive to extend further applications of Al alloys in engineering field, such as shipbuilding and oceanographic engineering.

KEYWORDS

5052 aluminum alloy, corrosion resistance, superhydrophobicity, passivation

INTRODUCTION

Aluminum and its alloys, as increasingly important engineering materials, have been widely used in various industrial fields including shipbuilding, oceanographic engineering, diving apparatus, architecture and machine manufacturing because of their low price, excellent machinability, high fatigue strength, low density, easy accessibility and environment friendly property[1-6]. However, they are easily penetrated and peeled owing to the corrosion destruction of their naturally formed protective surface oxide layers in seawater and solutions containing chloride ions[4, 7-9], which greatly shortens their service life and even brings enormous undesirable impact in the application fields, especially for the marine industries. Till now, many methods have been developed to protect aluminum and its alloys from corrosion in seawater, such as mechanical alloying[6, 10-12], electroplating coating[13-16], brush-plating coating[17, 18], magnetron sputtering ion coating[19-21], anodic oxidation[22-25], spray deposition technology[12, 26, 27] and laser surface technology[28-30], etc. Nevertheless, the reported approaches inevitably cause the environmental contamination and the fabricated processing is complex, high-cost and uncontrollable. Hence it is still a challenge to develop a facile approach to improve their corrosion resistance.

Inspired by the repelling water effect of lotus leaf, superhydrophobic surface has received great attentions in the past several decades[31-35]. In our previous researches, some superhydrophobic surfaces with excellent repelling water medium behaviors have been also presented via the fabrication of hierarchical micro/nano-scale structures on low surface energy metal substrates[36, 37]. Different from the hydrophilic solid surface, superhydrophobic substrates show a brand-new

substrate-air-water contacting interface, which offers a possibility to isolate metal substrates from the corrosive medium to improve their corrosion resistance. Initiated from this view, this approach has been employed to improve the corrosion resistance of aluminum and its alloys substrates through fabricating micro/nano-scale structures by some etchant firstly and then surface modification on their substrates[38-44]. For example, Escobar et al. has fabricated superhydrophobic surfaces with an improved corrosion resistance on pure commercial aluminum substrate by ethanol solution of hydrochloric acid etching and lauric acid modification[45]. Feng et al. have fabricated superhydrophobic surfaces with corrosion resistance on LD6063 aluminum alloy substrate by boiling water etching treatment and stearic acid modification[46]. However, few achievements were made about the prominent corrosion resistance of the fabricated aluminum and its alloys surfaces by the above classical two-step process.

As we know, metal passivation treatment can change the original surface activity of substrate making the electrode potential of metal turn to a positive direction, as a result, the substrate dissolution rate confront a rapidly falling trend and so is the case with corrosion rate. Herein, 5052 aluminum alloy substrates with superhydrophobicity and excellent corrosion resistance in 3.2 wt% sterile seawater have been fabricated via a simple and low-cost method of acid treatments and modification of fluoroalkyl-silane combined with surface passivation. First, large-scale hierarchical micro/nano-scale convex-concave structures on the surface of 5052 aluminum alloy have been prepared by hydrochloric acid etching after polishing treatment. Then, directly immersing the etched sample into potassium permanganate solution, as-prepared micro/nano-structures have been covered with the nano-scale flocculent passivation layer,

similar to the surface morphology of lotus leaf. Through optimizing the etching and passivation time, a superhydrophobic surface was attained after modification with Trichloro-(1H,1H,2H,2H-heptadecafluorodecyl) silane. Finally, the greatly improved corrosion resistance of the fabricated superhydrophobic surface was characterized by potentiodynamic polarization curves and electrochemical impedance spectroscopy. In addition, low adhesive behaviors of the fabricated surface have also been explored.

EXPERIMENTAL SECTION

Materials. The commercially available 5052 aluminum alloy sheets were purchased from Shanghai Haocheng Metal Ltd. Co. The main chemical compositions are 96.35 wt% aluminum and 2.5 wt% magnesium. Trichloro (1H,1H,2H,2H-heptadecafluorodecyl) silane (> 96%) was obtained from Tokyo Chemical Industry Ltd. Co. Other experimental chemicals used with analytic grade were purchased from Shanghai Chemical Reagent Ltd. Co. and also used as received without further treatment.

Etching processing. The aluminum alloy samples were prepared with a size of 10 mm × 10 mm × 1 mm. All samples were first polished manually in one direction with metallographic abrasive paper to roughen the surfaces for the desired durations. The sandpapers were fixed with a size of 50 mm × 50 mm and three types of #600, #1000, and #1200 grit sandpapers were used successively. The polished samples were cleaned with deionized (DI) water and ethanol for 10 min in the ultrasonic bath to remove the organic pollutants, respectively. After dried under a stream of N_2, they were etched by immersing into 4 M hydrochloric acid solution for 1, 2, 3, 4, 5,

6, 7, 8 and 10 min at room temperature, respectively. After acid etching, the obtained samples were immediately rinsed with DI water to stop the chemical reaction and washed to remove the remaining dust particles, then dried at 100 °C in an oven for 30 min.

Passivation processing. For their passivation, the etched aluminum alloy samples were placed into 0.1 M potassium permanganate solution for 60, 120, 180 and 240 min at room temperature, respectively. Then, they were rinsed with DI water and dried at room temperature.

Modification processing. The above fabricated aluminum alloy samples were modified by immersing into the ethanol solution of 20 mM Trichloro (1H,1H,2H,2H-heptadecafluorodecyl) silane for 12 h to attain a layer of perfluorosilane at room temperature. Then, they were dried at 100 °C in an oven for 1.5 h before further measurements.

Characterization. The contact angles (CAs) of droplets were measured on an OCA20 system equipped with a CCD camera and SCA 20 software from Dataphysics GmbH, Germany. The value of the static contact angle was recorded by employing 4 μL of distilled pure water droplets. Each contact angle was measured repeatedly at least five times at different positions of the aluminum alloy samples. The surface morphologies of as-prepared samples were observed by a Quanta 200 FEG Environmental scanning electronic microscopy (ESEM). The element composition was characterized by Oxford Instruments Inca X-Max energy dispersive X-ray (EDX) spectrometer associated with the FESEM instrument.

Electrochemical tests were characterized via potentiodynamic polarization curves and electrochemical impedance spectroscopy (EIS) by using a CHI660D electrochemical workstation (Shanghai Chen Hua Instrument Ltd. Co.) and a standard three-electrode system. The working

electrode was made of 5052 aluminum alloy sheet with the exposing area of 1 cm^2. The counter electrode is Pt net and reference electrode is saturated calomel electrode (SCE) with potential of 241 mV versus NHE at 25 °C. Working solution conducted at ambient temperature was 3.2 wt% sterile seawater, which must be boiled for 20 min. For potentiodynamic polarization measurements, the potential was taken between -1600 to -400 mV versus SCE with a scan rate of 1 $mV.s^{-1}$. EIS was measured under open circuit conditions in the frequency range between 10 mHz and 100 kHz with a sine-wave amplitude of 10 mV. One thing to be noted is that 30 min of immersion time was given before electrochemical tests to ensure steady state. All the measurement data reported are averages of three times repeated tests.

RESULTS AND DISCUSSION

Fabrication of superhydrophobic surface

Figure 1 shows the surface morphology of 5052 aluminum alloy samples after being polished with #600, #1000 and #1200 grit sandpapers successively and then etched with different time. The polished aluminum alloy surface is comparatively smooth besides some scratch defects with a fixed direction denoted by the red arrow in **Figure 1a**. **Figure 1b-f** exhibits the aluminum alloy surface morphology with the etching time of 2, 4, 6, 8 and 10 min, respectively. Evidently, many incompletable pits with micro-scale concave-convex structures emerge after being etched for 2 min. With the etching time increasing to 4 min, the etched surfaces become increasingly rough and the pits are almost interconnected throughout the entire surface. It is worth noting that large-scale labyrinth-like hierarchical concave-convex micro/nano-scale structures are covered

on the whole surface at the etching time of 6 and 8 min. Another point for concern is that the etching reaction is performed to a deeper layer of sample with the prolonging etching time, from which the layer boundaries are distinctly shown by red arrows in **Figure 1d-e**. With the etching time extending to 10 min, the regular hierarchical micro/nano-scale structures become more irregular and thin until the structures are dissolved and a fresh deeper layer of aluminum alloy substrate is exposed to the etchant. Another proof of the deeper layer etching phenomenon is the sample thickness variation with etching time prolonging, which will be explained in the following section. What is more, the cross-sectional view SEM images of the etching layers with the prolonging etching time are clearly demonstrated in **Figure S1** of the supplementary document. The etching evolution process revels that the etching layers are getting thicker and ultimately maintain at about 20 μm. Besides, these layers with the micro-scale concave-convex structures are observed to be hierarchical with numerous convex pits. A number of factors might account for the etched surface morphology. To begin with, a large number of line defects and dislocations exist in the crystal of aluminum alloy[40, 45, 47]. The dislocations could possess relatively high energy than other locations, which are more vulnerable to hydrochloric acid etchant. Additionally, some impurity atoms inevitably exist near the dislocation lines, which can intensify the etching reaction to some extent. The above two chemical active locations are preferentially dissolved by etchant and then fresh dislocations emerge. As a result, the etching reaction continues and large-scale hierarchical convex-concave micro/nano-scale structures are constructed on the surface of the aluminum alloy substrate.

The relationship between the etching time and the sample thickness as well as the sample wettability is presented in **Figure 2**. The sample thickness is measured by vernier caliper (500-196-20, Mitutoyo Corp., Japan) with the measurement accuracy of ±0.02 mm and resolution ratio of 0.01 mm. Then it averages after ten times sample thickness measurements at different positions of the aluminum alloy sample. All the data are measured at ambient temperature. Obviously, a hydrophobic substrate without acid treatments emerges with an average CA of 110±1.4° and the sample thickness of 1 mm after modified. However, CA would increase to 144±0.7°, 145±0.6°, 147±1.8° and 149±0.6° after the sample being immersed into the etchant for 1, 2, 3 and 4 min, respectively. Meanwhile, the thickness of the above four samples have barely changed and they still maintained at about 1 mm. When the etching time is extended to 5 min, a superhydrophobic surface demonstrates with an average CA of 153±0.5° but a decreasing ratio of sample thickness by 2%. Although all samples exhibit superhydrophobicity when the etching time is prolonged from 5 min to 10 min, the sample for 5 min achieves the maximal CA of 153±0.5°, from which the samples thickness conform to a decreasing law. As previously shown that the more extensively rough surface morphology emerges with the prolonging etching time, which could provide dislocation defects more opportunities of exposing to the etchant. As a result, the sample thickness is confronted with a sharp drop. After the etching time of 10 min, the sample thickness has already reduced by 14%, which can hardly meet economic demand for engineering materials despite the probable appearance of higher CAs. The inset in **Figure 2** corresponds to the aluminum alloy surface morphology demonstrating the

hierarchical convex-concave micro/nano-scale structures after being etched for 5 min. This morphology plays a key role on the superhydrophobicity of aluminum alloy surface.

Figure 3 shows the surface morphology evolution of the etched 5052 aluminum alloy samples for 5 min and then passivated for different time. As shown in **Figure 3a**, a spot of nanoparticles form on the etched hierarchical convex-concave micro/nano-scale structures of aluminum alloy surface with the passivation time of 60 min. With the passivation time prolonging to 120 min, the nanoparticles cumulate and the discontinuously flocculent structures form on the etched surface in **Figure 3b**. **Figure 3c-d** reveals the formation of more continuous large-scale nano-scale flocculent structures. The passivated nano-scale flocculent structures have barely changed the wettability of the etched hierarchical micro/nano-scale convex-concave structures on aluminum alloy surface. Obviously, the evidence could be founded by CAs after being modified, from which the average CAs achieve to 152±1.0°, 152±0.6°, 153±0.7° and 152±0.3° for the etched surfaces and then passivated for 60, 120, 180 and 240 min, respectively. All above fabricated surfaces exhibit superhydrophobicity. In fact, Cassie-Baxter equation demonstrates that the droplets on the fabricated superhydrophobic surfaces not only contact with the rough surfaces but also with the air trapped in the cavities of the fabricated rough structures, as shown in Eq.(1)[48]:

$$\cos\theta_{CA} = r\ f_1\ \cos\theta\ -\ f_2 \qquad (1)$$

where r is the roughness ratio of the wet surface area, f_1 refers to the surface fraction of a droplet contacting with solid surface, f_2 is the remaining surface fraction of a droplet contacting with air ($f_1 + f_2 = 1$), θ denotes the intrinsic contact angle of 110±1.4° for the surface after

modification but without etching treatment. When estimating f_1 and f_2, however, the roughness ratio of the wet surface area r is usually neglect, which can be seen in many works[38,42,45-47]. According to this equation, the samples after being etched for 5 min, passivated for 180 min and then modified (E5P180M) has got a CA of 153±0.7° demonstrating a droplet 85% contacting with air while only 15% with the discrete solid surface, which seems like a spherical droplet standing on the fabricated surface. Furthermore, the elementary substance of 5052 aluminum alloy surfaces with passivation treatment is further analyzed by EDX spectrum in **Figure 4**. Evidently, **Figure 4a** is primarily composed of O, Mg, Al and Cl, implying the existence of $AlCl_3$ as well as the oxidized layer on the surface after being etched for 5 min, which might be a result of the dissolve of the oxide film on aluminum alloy surface induced by Cl^- described as follows[40, 45, 47]:

$$Al_2O_3 + 6Cl^- + 6H^+ = 2AlCl_3 + 3H_2O \quad (2)$$

Besides, element Mg is from the inherent compositions of 5052 aluminum alloy substrate. After the etched sample being passivated for 180 min, element Mn is found besides Mg, Al and Cl, as shown in **Figure 4b**. The element Mn existing in the form of oxides comes from the potassium permanganate passivation process described as follows:

$$MnO_4^- + 4H^+ + 3e^- \rightarrow MnO_2 + 2H_2O \quad (3)$$

$$MnO_4^- + 2H_2O + 3e^- \rightarrow MnO_2 + 4OH^- \quad (4)$$

Among the passivation process, hydrogen ions are reduced but with the generation of more hydroxides. Furthermore, the chemical dehydration of these hydroxides will also produce more oxides.

To make further verification of the superhydrophobicity of 5052 aluminum alloy surface with E5P180M processing, an experiment about the adhesive property between the fabricated surface and a droplet (4 μL) is conducted, as shown in **Figure 5**. When it comes to E5P180M processing, the setting etching time of 5 min results from its maximal CA as explained in the previous section. Meanwhile, the setting passivation time of 180 min results from its optimal corrosion resistance, which will be explained in next section. During the whole contacting states, the droplet is adsorbed to the syringe needle fixed on an OCA20 system while the substrate keeps moving up and down. The original contact state exhibits a distance between the substrate and droplet. Consequently the droplet presents a natural appearance because of the gravity. The exact contact state reveals the same shape of the droplet as the original state with the substrate just touching it. When the substrate keeps rising, it may tightly and seriously contact with the droplet, from which the droplet is severely out of shape. It is worth noting that the same phenomenon is attained when the substrate departs from the droplet. Ultimately, when the substrate loses touch with the droplet absolutely, the droplet still keeps contacting with the immobile needle and the drop residue could not be detected on surface of the substrate in the last contact state. In summary, the adhesive performance between the fabricated surface and droplet is exceedingly weak and could be neglected. Based on above analysis, a simple and low-cost E5P180M processing can confirm 5052 aluminum alloy superhydrophobicity.

Corrosion resistance of fabricated superhydrophobic surface

The corrosion resistance property of 5052 aluminum alloy samples after being etched for 5 min and then passivated for different time is characterized by potentiodynamic polarization curves and corrosion current densities in 3.2 wt% sterile seawater at ambient temperature, as shown in **Figure 6**. It is believed that the preferable corrosion resistance results from the lower corrosion current density (I_{corr}) and the positive-going shift of the corrosion potential (E_{corr})[1,4,7]. Evidently, E_{corr} of the aluminum alloy samples shifts positively from -1.387 to -1.104 V with the prolonging passivation time before 180 min, as exhibited in potentiodynamic polarization curves in **Figure 6a**. Meanwhile, **Figure 6b** shows that I_{corr} obtained by the Tafel extrapolation method for samples with E5, E5P60, E5P120 and E5P180 processing is respectively 82.4, 37.59, 21.71 and 1.437 $\mu A.cm^{-2}$, which demonstrates an increasing corrosion resistance trend. It is important to reflect on the changes of the data. With the passivation time extending, the increasingly integrated nano-scale flocculent structures form and isolate substrates from the sterile seawater. Moreover, they can also increase opportunities of the air trapped in the fabricated multi-scale structures, which can play a role of the dielectric for a parallel plate capacitor and impede the ionic transfer process between electrolyte and aluminum alloy sample[49, 50]. The above ionic transfer process of electrochemical corrosion of the substrate in seawater can be described by anode reaction Eq.(5) and cathode reaction Eq.(6):

$$Al \rightarrow Al^{3+} + 3e^{-} \quad (5)$$

$$O_2 + 2H_2O + 4e^{-} \rightarrow 4OH^{-} \quad (6)$$

However, when the passivation time was prolonged to 240 min, data changes in the opposite direction on a small scale, which may be a result of the coverage of the etched hierarchical

micro/nano-scale structures induced by the excessively continuous and multilevel flocculent structures. As a matter of fact, the I_{corr} increases slightly from 1.437 μA.cm^{-2} for the sample with E5P180 processing to 4.073 μA.cm^{-2} with E5P240 processing demonstrating the marginally raised corrosion rate, which can be calculated by the corrosion resistance efficiency (IE) in Eq.(7)[4, 7]:

$$IE = 100\% \times (I_1 - I_2) / I_1 \quad (7)$$

where I_1 and I_2 are corrosion current densities of the surfaces of sample 1 and sample 2. IE means the corrosion resistance growth rate of sample 2 compared with sample 1. According to Eq.(7), IE of samples for E5P60, E5P120, E5P180 and E5P240 processing compared with sample for E5 processing is 54.4%, 73.7%, 98.3% and 95.1%, respectively. Distinctly, the etched sample passivated for 180 min has got the optimal corrosion resistance. It also has given the reason for the setting passivation time for 180 min in the test of adhesive performance mentioned above. In addition, the corrosion resistance can also be characterized by electrochemical impedance spectroscopy (EIS) and the corresponding Nyquist plots acquired for samples with E5, E5P60, E5P120, E5P180 and E5P240 processing are shown in **Figure 7**. For Nyquist plots, the semicircle represents the capacitance arc, which can reflect the value of the polarization resistance. Besides, large polarization resistance can impede the electron transfer process better. So a large semicircle diameter demonstrates a hard ionic transfer between the electrolyte and aluminum alloy sample, which indicates the superior corrosion resistance[4, 51]. Obviously, the same phenomenon about corrosion resistance ability with different treatments shown in potentiodynamic polarization curves could be found in EIS. In all, the corrosion resistance

property of 5052 aluminum alloy substrate is vastly improved with passivation treatment by immersing in 0.1 M potassium permanganate solution.

Figure 8 shows the potentiodynamic polarization curves and corrosion current densities characterizing the corrosion resistance property of the samples with M, E5M and E5P180M processing in 3.2 wt% sterile seawater at ambient temperature. **Figure 8b** represents I_{corr} of the above three samples acquired by the Tafel extrapolation method. Apparently, E_{corr} and I_{corr} of the aluminum alloy sample only with the modified processing are -1.139 V and 3.42 $\mu A.cm^{-2}$. Meanwhile, E_{corr} of samples shifts positively from -1.013 V for a two-step E5M processing to -0.952 V for E5P180M processing combined with the dropping I_{corr} from 1.377 $\mu A.cm^{-2}$ to 0.4413 $\mu A.cm^{-2}$. All these data indicate that the sample with E5P180M processing had the least chance to corrosion compared with the other two samples, which might be a result of the introduction of the passivation treatment. According to Eq.(7), IE of sample for E5P180M processing is improved by 68% compared with the traditional two-step E5M processing. Furthermore, when the corrosion resistance property of aluminum alloy samples with M, E5M and E5P180M processing is characterized by EIS, the same variation trend in potentiodynamic polarization curves can be investigated in **Figure 9**. The insert a), b) and c) are corresponded to photographs of wetting behaviors of aluminum alloy samples with M, E5M and E5P180M processing, respectively. Insert **a)** in **Figure 9** shows the photograph of 4 μL of liquid droplets dropping on the modified surface demonstrating a hydrophobic surface. The aluminum alloy surfaces treated with E5M and E5P180M both show extraordinary high repellency to droplets demonstrating two superhydrophobic surfaces in insert **b)** and **c)**. In brief, 5052 aluminum alloy

sample with innovative E5P180M processing has got the optimal corrosion resistance compared with traditional two-step E5M processing while still maintaining its superhydrophobicity.

Herein, how the perfluorosilane layer on the etched and passivated aluminum alloy surface forms and works to improve its corrosion resistance performance has also been investigated in **Figure 10**. **Figure 10a** shows the SEM image of the treated sample after being etched for 5 min, passivated for 180 min and then modified in the ethanol solution of 20 mM Trichloro (1H,1H,2H,2H-heptadecafluorodecyl) silane for 12 h. **Figure 10b** demonstrates the forming mechanism of the perfluorosilane layer on the etched and passivated aluminum alloy surface during the modification process. By immersing the treated aluminum alloy in the modification solution can produce the self-assembled perfluorosilane monolayer. Then, the perfluorosilane layer can be introduced by drying at 100 °C in an oven for 1.5 h. As we know that the fluorine atom has strong polarity and electron-withdrawing effect, which can make C-F bond a strong chemical inertness. As a result, perfluorosilane layer shows very low surface energy, which can repel the water and some other corrosion medium. Meanwhile, its CH groups have a good ability of anti-OH bonds[41], which can intensify the above repelling ability. Due to the above effects, the perfluorosilane layer guarantees its superior anti-corrosion performance.

CONCLUSIONS

Superhydrophobic 5052 aluminum alloy substrates with an excellent corrosion resistance have been successfully prepared by a simple and low-cost method of acid treatments and modification of fluoroalkyl-silane combined with surface passivation. By adjusting the etching time with

hydrochloric acid and the passivation time with potassium permanganate, the large-scale superhydrophobic surface morphology of the hierarchical convex-concave micro/nano-structures combining with nano-scale flocculent structures could be finely manipulated on surface of aluminum alloy substrate, which accounts for the superior wettability and prominent corrosion resistance. For the fabricated surface achieved by an etching processing with 4 M hydrochloric acid for 5 min and a passivation processing with 0.1 M potassium permanganate for 180 min, it stands for the optimal superhydrophobic performance with a contact angle of 153±0.7° for a 4 μL of water droplet after the surface modification. Furthermore, the fabricated superhydrophobic surface shows an extremely weak adhesive force to water droplet. When it comes to the corrosion resistance, passivation with potassium permanganate has exactly reduced the corrosion rate of aluminum alloy sample, for the increasing corrosion resistance efficiency of 98.3% of the E5P180 processing sample compared with E5 processing. Meanwhile, compared with traditional two-step E5M processing, the corrosion resistance efficiency with the innovative E5P180M processing is improved by 68%.

ACKNOWLEDGMENT

This work was supported by the National Key Scientific Program-Nanoscience and Nanotechnology (2011CB933700), and National Natural Science Foundation of China (51210008). X.J.H. acknowledges the CAS Institute of Physical Science, University of Science and Technology of China (2012FXCX008), for financial support.

Figure captions:

Figure 1. SEM images of aluminum alloy surface morphology after being a) polished with #600, #1000, and #1200 grit sandpapers successively; b), c), d), e) and f) etched with 4 M hydrochloric acid for 2, 4, 6, 8 and 10 min, respectively. The insets corresponding to the magnified images. The red arrow in a) pointing to the polishing direction, while in d) and e) pointing to layer boundaries.

Figure 2. Effects of etching time in the 4 M hydrochloric acid on the samples thickness and the wettability of the fabricated surfaces after modification. The inset corresponding to surface morphology of the hierarchical convex-concave micro/nano-scale structures with etching time of 5 min.

Figure 3. SEM images of aluminum alloy surface morphology passivated for a) 60 min, b) 120 min, c) 180 min and d) 240 min after being etched for 5 min. The insets corresponding to CA of the fabricated surfaces after being modified.

Figure 4. EDX spectrum of 5052 aluminum alloy surfaces with the treatment of a) etched for 5 min and b) passivated for 180 min after being etched for 5 min.

Figure 5. A series of photos about the aluminum alloy substrates making different contacting states with a droplet corresponding to the fabricated surfaces with E5P180M processing. The red arrow referring to moving direction of aluminum alloy sample.

Figure 6. a) and b) respectively referring to potentiodynamic polarization curves and corrosion current densities of samples after being etched for 5 min (E5), etched for 5 min and then passivated for 60 min (E5P60), etched for 5 min and then passivated for 120 min (E5P120), etched for 5 min and then passivated for 180 min (E5P180), etched for 5 min and then passivated for 240 min (E5P240) at room temperature in 3.2 wt% sterile seawater.

Figure 7. Nyquist plots of samples with E5, E5P60, E5P120, E5P180 and E5P240 processing at room temperature in 3.2 wt% sterile seawater.

Figure 8. a) and b) respectively referring to potentiodynamic polarization curves and corrosion current densities of samples after being modified (M), etched for 5 min and then modified (E5M) and also with E5P180M processing immersed in 3.2 wt% sterile seawater at room temperature.

Figure 9. Nyquist plots of aluminum alloy samples immersed in 3.2 wt% sterile seawater at room temperature and underwent the treatment of M, E5M and E5P180M. The insert corresponding to photographs of 4 μL liquid droplets dripping on aluminum alloy surfaces with treatment of a) M, b) E5M and c) E5P180M.

Figure 10. a) corresponding to the SEM image of the treated aluminum alloy sample after being etched for 5 min, passivated for 180 min and then modified in the ethanol solution of 20 mM Trichloro (1H,1H,2H,2H-heptadecafluorodecyl) silane for 12 h. b) illustrating the forming mechanism of the perfluorosilane layer on the etched and passivated aluminum alloy surface during the immersing modification process.

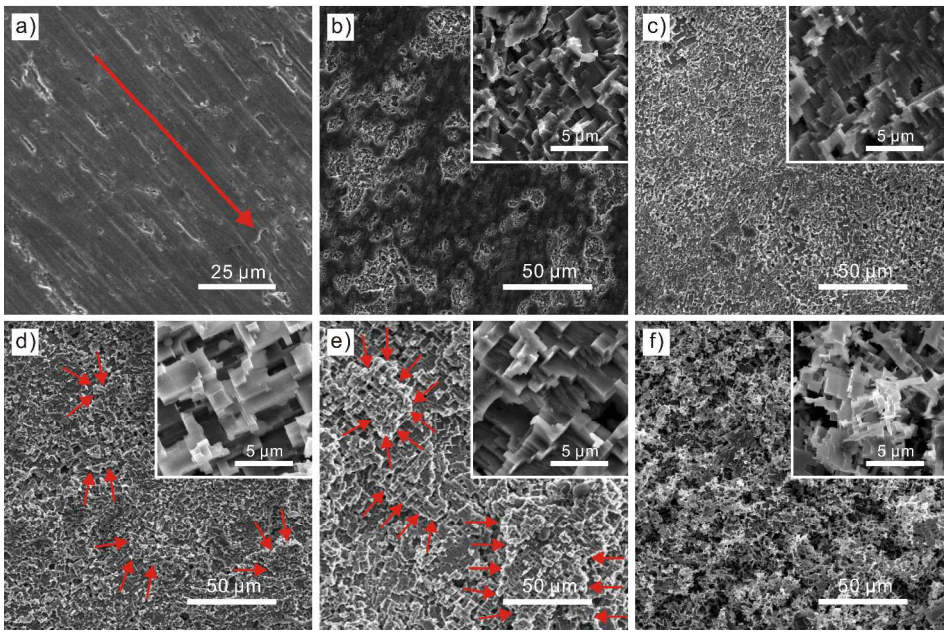

Figure 1. SEM images of aluminum alloy surface morphology after being a) polished with #600, #1000, and #1200 grit sandpapers successively; b), c), d), e) and f) etched with 4 M hydrochloric acid for 2, 4, 6, 8 and 10 min, respectively. The insets corresponding to the magnified images. The red arrow in a) pointing to the polishing direction, while in d) and e) pointing to layer boundaries.

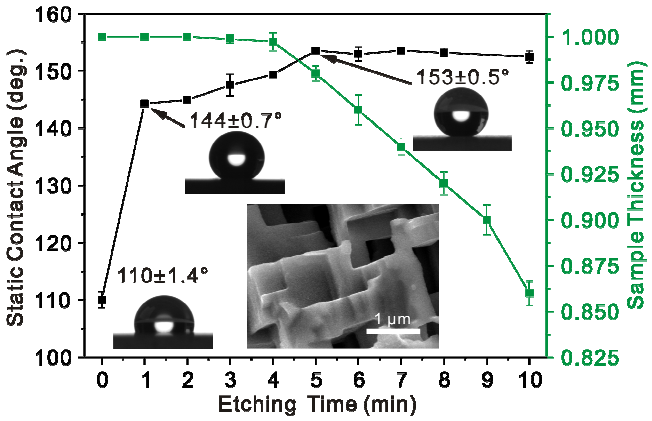

Figure 2. Effects of etching time in the 4 M hydrochloric acid on the samples thickness and the wettability of the fabricated surfaces after modification. The inset corresponding to surface morphology of the hierarchical convex-concave micro/nano-scale structures with etching time of 5 min.

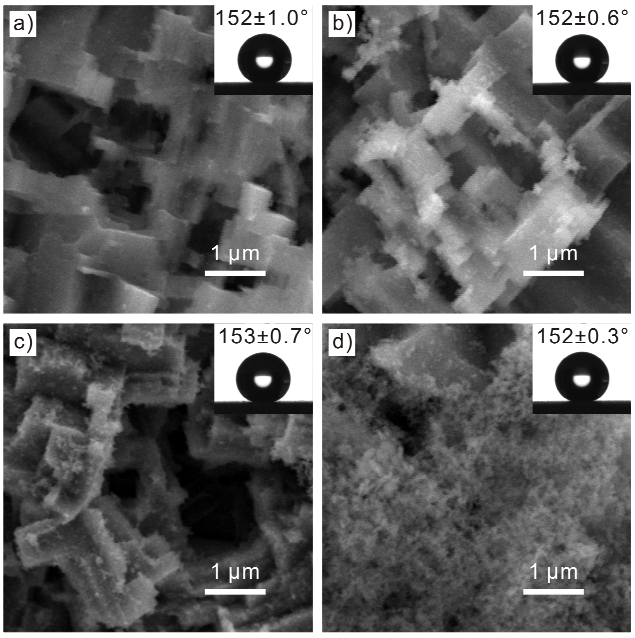

Figure 3. SEM images of aluminum alloy surface morphology passivated for a) 60 min, b) 120 min, c) 180 min and d) 240 min after being etched for 5 min. The insets corresponding to CA of the fabricated surfaces after being modified.

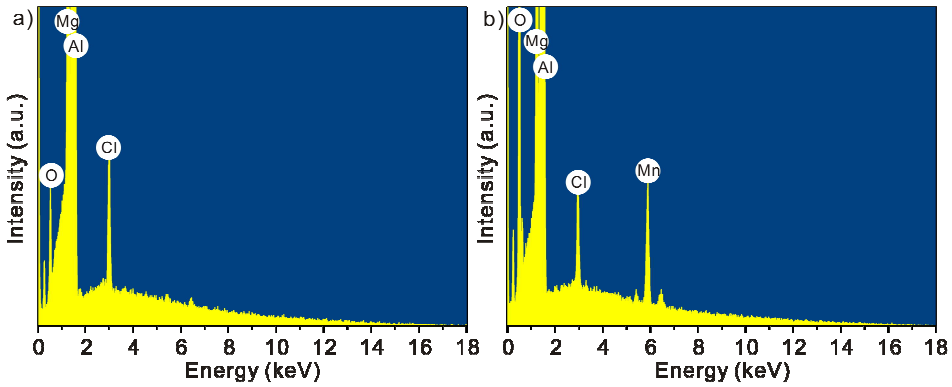

Figure 4. EDX spectrum of 5052 aluminum alloy surfaces with the treatment of a) etched for 5 min and b) passivated for 180 min after being etched for 5 min.

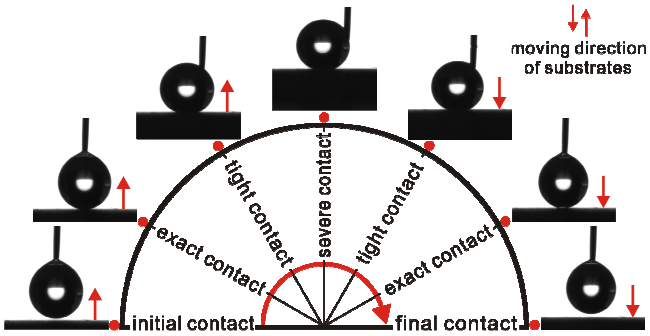

Figure 5. A series of photos about the aluminum alloy substrates making different contacting states with a droplet corresponding to the fabricated surfaces with E5P180M processing. The red arrow referring to moving direction of aluminum alloy sample.

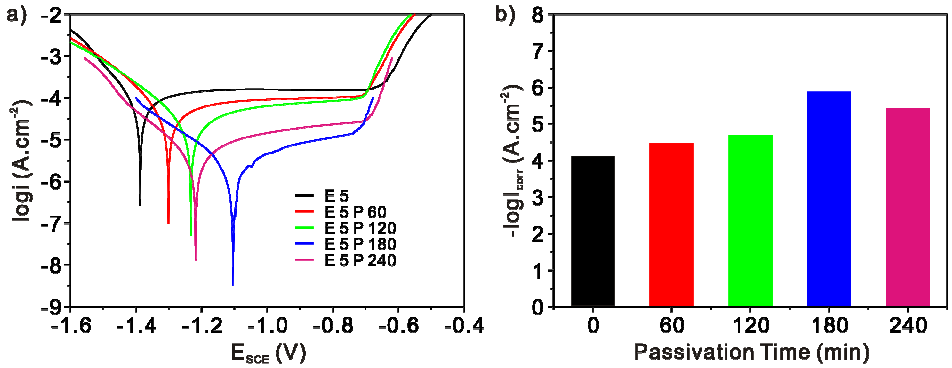

Figure 6. a) and b) respectively referring to potentiodynamic polarization curves and corrosion current densities of samples after being etched for 5 min (E5), etched for 5 min and then passivated for 60 min (E5P60), etched for 5 min and then passivated for 120 min (E5P120), etched for 5 min and then passivated for 180 min (E5P180), etched for 5 min and then passivated for 240 min (E5P240) at room temperature in 3.2 wt% sterile seawater.

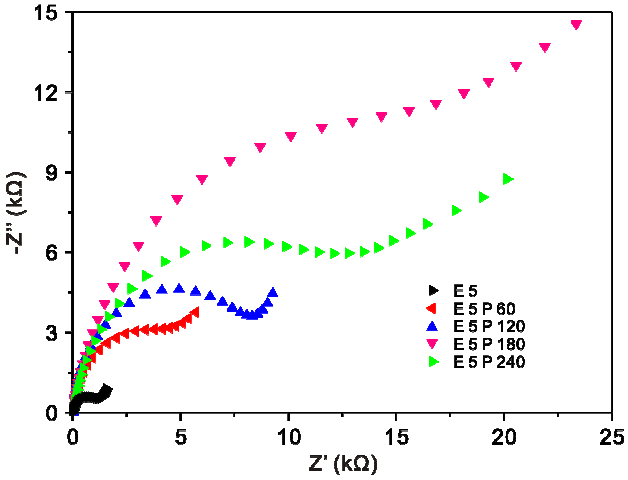

Figure 7. Nyquist plots of samples with E5, E5P60, E5P120, E5P180 and E5P240 processing at room temperature in 3.2 wt% sterile seawater.

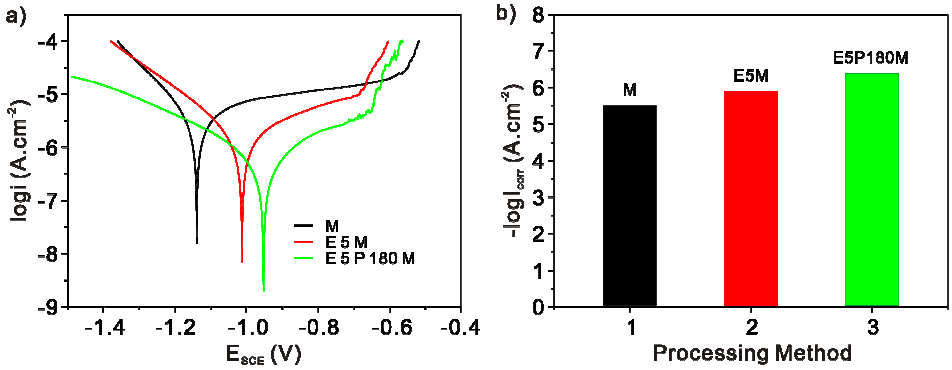

Figure 8. a) and b) respectively referring to potentiodynamic polarization curves and corrosion current densities of samples after being modified (M), etched for 5 min and then modified (E5M) and also with E5P180M processing immersed in 3.2 wt% sterile seawater at room temperature.

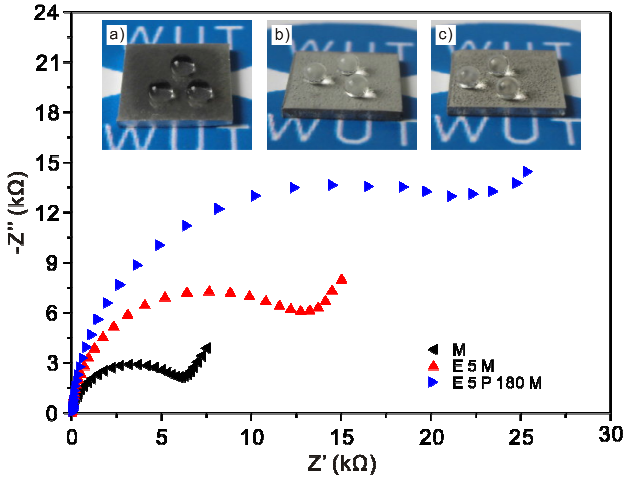

Figure 9. Nyquist plots of aluminum alloy samples immersed in 3.2 wt% sterile seawater at room temperature and underwent the treatment of M, E5M and E5P180M. The insert corresponding to photographs of 4 μL liquid droplets dripping on aluminum alloy surfaces with treatment of a) M, b) E5M and c) E5P180M.

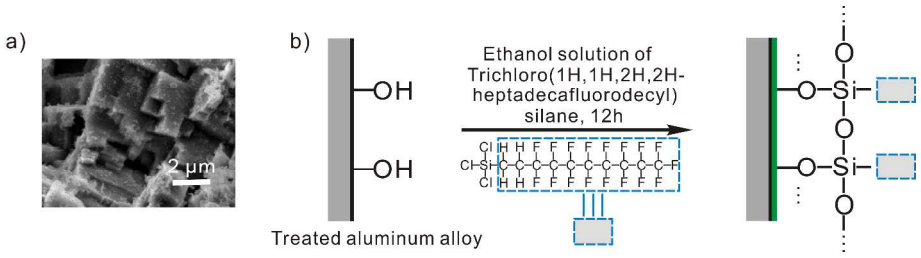

Figure 10. a) corresponding to the SEM image of the treated aluminum alloy sample after being etched for 5 min, passivated for 180 min and then modified in the ethanol solution of 20 mM Trichloro (1H,1H,2H,2H-heptadecafluorodecyl) silane for 12 h. b) illustrating the forming mechanism of the perfluorosilane layer on the etched and passivated aluminum alloy surface during the immersing modification process.

REFERENCES

1. Y. S. Huang, T. S. Shih and J. H. Chou, *Applied Surface Science*, 2013, **283**, 249-257.
2. M. Liu, P. Schmutz, S. Zanna, A. Seyeux, H. Ardelean, G. Song, A. Atrens and P. Marcus, *Corrosion Science*, 2010, **52**, 562-578.
3. S. H. Park, J. S. Kim, M. S. Han and S. J. Kim, *Transactions of Nonferrous Metals Society of China*, 2009, **19**, 898-903.
4. Y. S. Yin, T. Liu, S. G. Chen, T. Liu and S. Cheng, *Applied Surface Science*, 2008, **255**, 2978-2984.
5. J. L. Song, W. J. Xu, X. Liu, Y. Lu, Z. F. Wei and L. B. Wu, *Chemical Engineering Journal*, 2012, **211-212**, 143-152.
6. E. S. M. Sherif, H. R. Ammar and K. A. Khalil, *Applied Surface Science*, 2014, **301**, 142-148.
7. Z. L. Chen, M. B. Shuai and L. D. Wang, *Journal of Solid State Electrochemistry*, 2013, **17**, 2661-2669.
8. S. Gudic, I. Smoljko and M. Kliskic, *Journal of Alloys and Compounds*, 2010, **505**, 54-63.
9. D. J. Shen, G. L. Li, C. H. Guo, J. Zou, J. R. Cai, D. L. He, H. J. Ma and F. F. Liu, *Applied Surface Science*, 2013, **287**, 451-456.
10. M. S. Zou, X. Y. Guo, H. T. Huang, R. J. Yang and P. Zhang, *Journal of Power Sources*, 2012, **219**, 60-64.
11. J. Abenojar, A. Bautista, S. Guzman, F. Velasco and M. A. Martinez, *Materials and Corrosion-Werkstoffe Und Korrosion*, 2014, **65**, 678-684.
12. Y. L. Cheng, Z. H. Chen, H. L. Wu and H. M. Wang, *Materials and Corrosion-Werkstoffe Und Korrosion*, 2007, **58**, 280-284.
13. A. E. Fetohi, R. M. A. Hameed and K. M. El-Khatib, *Journal of Power Sources*, 2013, **240**, 589-597.
14. A. L. M. Carvalho and H. J. C. Voorwald, *International Journal of Fatigue*, 2007, **29**, 1282-1291.
15. A. E. Fetohi, R. M. A. Hameed, K. M. El-Khatib and E. R. Souaya, *International Journal of Hydrogen Energy*, 2012, **37**, 7677-7688.
16. C. S. Dai, D. L. Wang, X. G. Hu and K. Wang, *Plating and Surface Finishing*, 2004, **91**, 34-39.
17. Z. Z. Han, Y. Zuo, P. F. Ju, Y. M. Tang, X. H. Zhao and J. L. Tang, *Surface & Coatings Technology*, 2012, **206**, 3264-3269.
18. J. L. Tang, Z. Z. Han, Y. Zuo and Y. M. Tang, *Applied Surface Science*, 2011, **257**, 2806-2812.
19. B. Zhang, Y. Li and F. H. Wang, *Corrosion Science*, 2007, **49**, 2071-2082.
20. S. A. Umoren, Y. Li and F. H. Wang, *Journal of Applied Electrochemistry*, 2011, **41**, 307-315.
21. F. Y. Zhang and M. F. Yan, *Vacuum*, 2014, **103**, 87-92.
22. E. Matykina, R. Arrabal, A. Pardo, M. Mohedano, B. Mingo, I. Rodriguez and J. Gonzalez, *Materials Letters*, 2014, **127**, 13-16.
23. J. Ryl, J. Wysocka, M. Jarzynka, A. Zielinski, J. Orlikowski and K. Darowicki, *Corrosion Science*, 2014, **87**, 150-155.
24. S. B. Madden and J. R. Scully, *Journal of the Electrochemical Society*, 2014, **161**, C162-C175.
25. W. Yang, B. L. Jiang, H. Y. Shi and L. Y. Xian, *J. Cent. South Univ. Technol.*, 2010, **17**, 223−227.
26. M. Hasan, J. Stokes, L. Looney and M. S. J. Hashmi, *Surface & Coatings Technology*, 2008, **202**, 4006-4010.

27. F. Andreatta, L. Paussa, P. Aldighieri, A. Lanzutti, D. Ondratschek and L. Fedrizzi, *Surface and Interface Analysis*, 2010, **42**, 293-298.
28. A. Gisario, M. Barletta and F. Veniali, *Optics and Laser Technology*, 2012, **44**, 1942-1958.
29. T. Sugihara and T. Enomoto, *Precision Engineering-Journal of the International Societies for Precision Engineering and Nanotechnology*, 2012, **36**, 229-237.
30. Y. Sano, K. Akita, K. Masaki, Y. Ochi, I. Altenberger and B. Scholtes, *Journal of Laser Micro Nanoengineering*, 2006, **1**, 161-166.
31. H. Q. Liu, S. Szunerits, W. G. Xu and R. Boukherroub, *ACS applied materials & interfaces*, 2009, **1**, 1150-1153.
32. A. Ahuja, J. A. Taylor, V. Lifton, A. A. Sidorenko, T. R. Salamon, E. J. Lobaton, P. Kolodner and T. N. Krupenkin, *Langmuir*, 2008, **24**, 9-14.
33. Y. T. Cheng, D. E. Rodak, C. A. Wong and C. A. Hayden, *Nanotechnology*, 2006, **17**, 1359-1362.
34. N. J. Shirtcliffe, G. McHale, M. I. Newton and Y. Zhang, *ACS applied materials & interfaces*, 2009, **1**, 1316-1323.
35. T. Liu, S. G. Chen, S. Cheng, J. T. Tian, X. T. Chang and Y. S. Yin, *Electrochimica Acta*, 2007, **52**, 8003-8007.
36. Q. X. Zhang, Y. X. Chen, Z. Guo, H. L. Liu, D. P. Wang and X. J. Huang, *ACS applied materials & interfaces*, 2013, **5**, 10633-10642.
37. Z. Guo, X. Chen, J. Li, J. H. Liu and X. J. Huang, *Langmuir*, 2011, **27**, 6193-6200.
38. L. Yin, Y. Y. Wang, J. F. Ding, Q. J. Wang and Q. M. Chen, *Applied Surface Science*, 2012, **258**, 4063-4068.
39. D. G. Xie and W. Li, *Applied Surface Science*, 2011, **258**, 1004-1007.
40. B. T. Qian and Z. Q. Shen, *Langmuir*, 2005, **21**, 9007-9009.
41. M. Ruan, W. Li, B. S. Wang, Q. Luo, F. M. Ma and Z. L. Yu, *Applied Surface Science*, 2012, **258**, 7031-7035.
42. S. Ji, P. A. Ramadhianti, T. B. Nguyen, W. D. Kim and H. Lim, *Microelectronic Engineering*, 2013, **111**, 404-408.
43. S. Q. Liang, R. M. Wu, Z. Q. Yuan, H. Chen and Y. Yu, *Procedia Engineering*, 2012, **27**, 1752-1757.
44. R. M. Wu, S. Q. Liang, Z. Q. Yuan, H. Chen and J. Deng, *Advanced Materials Research*, 2011, **160-162**, 379-383.
45. A. M. Escobar and N. Llorca-Isern, *Applied Surface Science*, 2014, **305**, 774-782.
46. L. B. Feng, Y. H. Che, Y. H. Liu, X. H. Qiang and Y. P. Wang, *Applied Surface Science*, 2013, **283**, 367-374.
47. Y. F. Zhang, J. Wu, X. Q. Yu and H. Wu, *Applied Surface Science*, 2011, **257**, 7928-7931.
48. A. B. D. Cassie and S. Baxter, *Transactions of the Faraday Society*, 1944, **40**, 546-551.
49. Z. J. Wang, J. H. Gong, J. H. Ma and J. Xu, *RSC Advances*, 2014, **4**, 14708.
50. L. J. Liu, F. Y. Xu, Z. L. Yu and P. Dong, *Applied Surface Science*, 2012, **258**, 8928-8933.
51. S. Joshi, W. G. Fahrenholtz and M. J. O'Keefe, *Surface and Coatings Technology*, 2011, **205**, 4312-4319.